Journal of Computational Physics 239 (2013) 57–71

Contents lists available at SciVerse ScienceDirect

Journal of Computational Physics

journal homepage: www.elsevier.com/locate/jcp

# Lattice Boltzmann method for simulations of gas-particle flows over a backward-facing step

Haoming Wang, Haibo Zhao *, Zhaoli Guo, Yongxiang He, Chuguang Zheng

*State Key Laboratory of Coal Combustion, Huazhong University of Science and Technology, Wuhan, 430074 Hubei, People's Republic of China*

ARTICLE INFO

*Article history:*
Received 21 May 2012
Received in revised form 22 November 2012
Accepted 22 December 2012
Available online 10 January 2013

*Keywords:*
Lattice Boltzmann method
Lattice gas automata
Gas–solid flows
Two-way coupling
Backward-facing step flows

ABSTRACT

The simulation of turbulent gas–solid flows at the mesoscopic scale is still challenging in fluid mechanics. This paper proposed the Lattice Boltzmann-cellular automata (LB-CA) probabilistic model to simulate gas–solid flows, in which the two-way coupling between the carrier phase and the dispersed phase is considered. In the LB-CA model, the LB subgrid model for high Reynolds number flows is used to describe flow fields at the mesoscopic scale, and the CA probabilistic model utilizing the stochastic process is used to capture transport behavior of discrete solid particles among the same regular lattice nodes as fictitious fluid particles in the LB method. The transport probability of a solid particle to nearest neighboring node directly depends on its actual displacement under other external forces (e.g., drag force, gravity). The two-way coupling is realized by adding external force term for the feedback forcing of particles in the evolution equation of fluid particle density distribution function. The resultant LB-CA model with two-way coupling is then used to simulate gas-particle flows over a backward-facing step. By comparing the present results with experimental measurements and other simulation results from LES (large-eddy simulation)-Lagrangian model, LB-Lagrangian model and two-fluid model, it is found that the LB-CA model is capable of simulating mean and fluctuating velocities of the carrier and dispersed phases and gas-particle covariance with high precision. Generally, the LB-CA method achieves the similar precision with the LES-Lagrangian method, and performs better than some other macroscopic models (such as the two-fluid models).



## 1. Introduction

Gas–solid two-phase flow often occurs in nature and engineering, such as pulverized-coal particle transport, jetting and combustion in boilers/gasifiers, fly ash transport and deposition in flue gas and diffusion and sedimentation in atmospheric environment [1]. Particle-laden flows in engineering almost belong to turbulent two-phase flows, containing various vortexes ranged from Kolmogorove scale to integral scale [2,3]. The vortexes of continuous phase play an important role in particle transport, therefore the interaction between particles and vortexes has become an important task in turbulent two-phase flows. The gas–solid flow models have gradually popularized from one-way coupling (only drag force acting on particles is taken into account) to two-way coupling (considering also the back influence of the dispersed phase on the carrier-phase dynamics), and further to four-way coupling (considering further the interactions between particles such as collision, agglomeration, and fragmentation).

* Corresponding author. Tel.: +86 27 87545526x8208; fax: +86 27 87545526.
*E-mail address:* klinsmannzhb@163.com (H. Zhao).

0021-9991/$ - see front matter © 2013 Elsevier Inc. All rights reserved.
http://dx.doi.org/10.1016/j.jcp.2012.12.032

The gas–solid flow models are usually distinguished between two-fluid models (Eulerian–Eulerian models) and fluid-trajectory models (Eulerian–Lagrangian models). Generally speaking, the Eulerian–Lagrangian models are at advantages of considering particle–fluid interaction, particle–particle interaction, and multicomponent and polydispersed particles because they are able to obtain the detailed information on history, trajectory crossing, and internal structure of particles. However, for conventional models the gas–solid flow fields are computed only at the macroscale, especially the details of the gas flow at the microscale (of the order of a particle size) are approximately modeled rather than directly depicted [4]. In fact, it is difficult for the widely-used turbulence model theory (such as approaches based on Reynolds-Averaged Navier–Stokes (RANS) equations) to consider the effects of vortex structure and the transformation of vortex [5]. On the other side, Direct Numerical Simulation (DNS) is able to accurately describe turbulence structure even for turbulent flows with moderate Reynolds number, however on the cost of huge computational demand. In addition, if the turbulence models are based on the Navier–Stokes equations, it means the continuous medium hypothesis is adopted and then the models cannot be applied in the simulation of flow behavior in the transition regime, in the free molecular regime, and even in the slip flow regime. Therefore, the key issues developing an exact model to simulate the gas–solid flow include at least: (1) an exact fluid model which can capture detailed information of carrier-phase turbulence and deal with complex boundary condition; (2) an appropriate particle motion model which can describe the complex rheology of dispersed phase; (3) a model for one-, two-, or four-way coupling between the phases, depending on the fractional volume occupied by the dispersed phase ($\Phi_v$) and the mass loading ($\Phi_m$).

In order to simulate flow field at the mesoscopic or microscopic level, expensive computational cost is required for these fully-resolved methods such as molecular dynamics (MD) simulation, kinetic theory of gases (e.g., Boltzmann equation method and direct simulation Monte Carlo (DSMC)) and DNS. An important way to reduce computational cost of microscopic/mesoscopic models is to simplify physical picture of molecular motion as far as possible. Cellular Automata (CA), Lattice Gas Automata (LGA) and Lattice Boltzmann (LB) methods are all based on this idea and have been successively developed since 1980s. These lattice-based methods simulate continuous fluid at the macroscale in terms of the dynamics of discrete fictitious "fluid particles" at a mesoscopic level, and the macroscopic features of flows can be obtained through the statistics of many discrete fluid particles, which transport between regular grid points and collide with each other. The lattice-based methods have got extensive attention and have been well developed to simulate complex flows because of their inherent advantages of clear physical picture, simplicity, intrinsic parallelism, and capability to deal with complex and dynamic boundary conditions. Based on kinetic theory of gases, the LB method tracks the evolution of fluid-particle density distribution function rather than fluid-particle number density in the LGA and CA methods [6]. The LB method is thus capable of overcoming statistics noise inherent to the LGA and CA and achieving quasi linear complexity of collision operator. Furthermore, the LB method has more degrees of freedom (e.g., fluid viscosity is free variable in the LB but determined by collision rules in the LGA) and more efficient than the LGA and CA. Up to now, the LB has gradually replaced the LGA and CA in simulations of flow fields [7]. However, it is worth noting that the LGA and CA methods also exhibit particular advantages. For example, the LGA and CA methods track Boolean variable which is always nonnegative, they thus performs better numerical stability than the LB; Unlike the LGA and CA methods, the LB, which is originated from the Boltzmann equation and based on the molecular chaos hypothesis, cannot consider multi-body collision and keep track of the correlations between the particles and, accordingly, the microscopic fluctuation of fluid [8]. In this paper, the LB is selected to simulate turbulent carrier-phase flows and an idea similar to the LGA and CA is used in the simulation of solid particle motion.

Depending on different ways for description of particle motion (Lagrangian tracking or probabilistic determination) and particle volume (full resolution or point like), there are three kinds of gas–solid models based on the LB method, namely, Lagrangian point-like particle tracking approach, Lagrangian fully-resolved particle tracking approach, and cellular automata probabilistic approach. The Lagrangian point-like particle tracking approach (we call it the LB-Lagrangian approach in the following text) views solid particle as point without volume, and the motion of each particle is directly calculated from the Lagrangian approach of the equation of motion under consideration of different external forces such as drag force and gravity. The point-particle assumption is reasonable when the particles are smaller than the Kolmogorov scale of fluid phase [4]. The approach is successfully utilized to simulate particle deposition in filters [9,10] and particle-laden flows over a backward-facing step [11,12]. However, it is worth noting that the LB-Lagrangian approach may lose the parallelism inherent to the LB methods and be trapped into the coupling between fluid particles and solid particles, because the two kinds of particles are not based on the same lattices.

The second Lagrangian particle tracking approach views solid particle as objects with geometric boundaries imposed on the fluid. The interaction between a "large" solid particle and its surrounding fluid particles is calculated by summing the transfer of momentum to the solid boundary (before and after rebound [13]) over all fluid boundary nodes [7]. The approach is capable of describing complex rheology of particle suspensions with high resolution, and then exploring complex fluid–particle interaction from the viewpoint of "true" DNS and providing basic parameters and even constitutive relations for macroscopic simulation. However, the approach is generally trapped into huge computational demand in cases of, for example, 10,000 particles in suspensions [7], and thus is still out of the engineering question nowadays.

The cellular automata probabilistic approach, which was firstly proposed by Masselot and Chopard [14–17] for particle (such as snow or sand) behavior in fluid (typically, air and water), is based on the following ideas: the discrete point-like particles are constrained to exist only at the same regular lattice nodes as the fluid particles of the LB; the state of a solid particle at a node is expressed by a Boolean variable (as those in the CA [18] and LGA [19]), and an arbitrary number of point particles may exist at each node; During a time-step, a solid particle at a node may still stay at the original node or migrate to

its nearest-neighbor node, depending on the transport probability of the particle which is determined by the combined effect of, for example, gravity and drag force. The approach is thus called cellular automata probabilistic approach. Because "continuous" fluid and discrete granular media are modeled in terms of fluid particles and solid particles using the same lattices, this approach is at advantages of the convenient implementation of dynamic boundary conditions, massively parallel computation, and complicated microscopic mechanisms of solid particles (e.g., deposition, toppling, and erosion). Chopard and his colleagues used the mixed LB and CA approach (we note it LB-CA method in the following text) to describe transport (creeping, saltation, and suspension), deposition, toppling, and erosion of snow particles in air [15], as well transport, erosion, and deposition of sands in water [14–16]. Gradoń and his colleagues extended the LB-CA method to describe transport, deposition, and resuspension of particular matter in fibrous filters [20,21]. Although the LB-CA method provides a way to incorporate these complex mechanisms for particle behaviors by some simple and intuitive rules, these rules are characterized by empirical or tentative formulations/parameters. For example, an empirical constant for the ratio of particle velocity and fluid velocity is set to determine the transport probability of a particle under the action of the local fluid flow [14,15,20,21]. In the case, the influence of fluid on particle motion is described by a less rigorous or even wrong model. Through choosing appropriate characteristic parameters for particle behavior very carefully, the LB-CA method can obtain some reasonable pattern of particle-laden flows. However, these empirical formulations/parameters adopted in the LB-CA method make it be only on the level of qualitative simulation. Recently, we [22] established a model for particle transport probabilities by quantitatively calculating the velocity and displacement of solid particles under the combined effect of, for example, drag force from local fluid and Brownian diffusion. The improved LB-CA method is further utilized to simulate steady-state filtration process of clear fibers and non-steady-state filtration process during filter loading for different typical cases where either individual collection mechanism (e.g., Brownian diffusion, or interception, or inertial impaction) or simultaneous several mechanisms dominate the filtration process. The simulation results for capture efficiency and pressure drop are in good agreement with previous theoretical predictions and experimental observations. However, in the LB-CA method, only one-way coupling between the two phases was taken into account and the feedback forcing of solid particles acting on fluid particles was neglected. The one-way coupling for multiphase flow simulation is reasonable when the fractional volume and mass loading of particles are small (e.g., $\Phi_v < 10^{-6}$). However when $\Phi_v$ increases or when the phenomenon of preferential accumulation results in obvious nonuniform distribution of particles, the effect of the turbulent carrier flow on the dynamics of the dispersed phase and the back influence of the dispersed phase on the carrier-phase dynamics should be considered simultaneously (*i.e.*, the two-way coupling between the two phases).

This paper aims to establish the two-way coupled LB-CA method for gas-particle flows and it is organized as follows. In Section 2, the *D*2*Q*9 model with BGK collision operator was introduced to simulate the flow field. Meanwhile, the Smagorinsky subgrid model was introduced to describe the turbulent flow with high Reynolds number. Section 3 presented the CA probabilistic model for particle transport under the consideration of drag force and gravity. In Section 4, the interaction between the phases was realized by adding external force term in the evolution equation of fluid-particle density distribution function. Section 5 introduced the boundary conditions in brief. In Section 6, we first verified the CA probabilistic model for particle transport by comparing it with the Lagrange tracking approach. Then the LB-CA method is used to simulate particle-laden flow over a backward facing step, and velocity profiles (mean velocity and fluctuating velocity) of both phase and gas–solid covariance were obtained and compared with available experimental data and simulation results of other models. Finally, conclusions are given in Section 7.

## 2. The Lattice-Boltzmann method for the carrier-phase turbulence

In this paper the two-dimensional flow fields are first calculated using the LB method, where the classical *D*2*Q*9 model (in term of latticle-BGK (Bhatnagar–Gross–Krook) model [23]) is adopted. In the LB method, a fictitious microscopic picture of

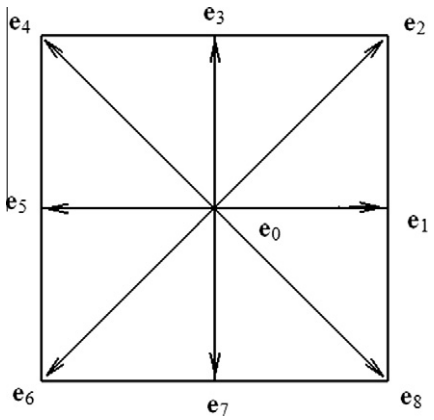


**Fig. 1.** Discrete velocities in the *D*2*Q*9 Lattice Boltzmann model.

molecular dynamics for the fluid phase is imaged, where a discrete regular grid (lattice) in space, an explicit time-stepping in time, and discrete velocities of hypothetical fluid particles are adopted. Fig. 1 presents the nine discrete velocities in the *D*2*Q*9 model. Hypothetical fluid particles are constrained to move only along the links of some regular lattices and collide at the nodes. The fluid-particle probability density distribution function $f_i(\mathbf{x},t)$, which represents the probable amount of fluid particles moving with a fixed velocity $\mathbf{c}_i$ along the $i$th direction at each node with position $\mathbf{x}$ and at discrete time $t$, is concerned. Each $f_i$ corresponds to a certain velocity vector $\mathbf{c}_i$ ($i = 0,\ldots,8$ in the *D*2*Q*9 model). The carrier-phase dynamics is simulated by the collision and streaming of "fictitious" fluid particles in term of the evolution of $f_i(\mathbf{x},t)$. Fictitious fluid particles collide and migrate in each time step $\Delta t$, here we use BGK collision operator to deal with particle collision [23]:

$$f_i^+(x,t) = f_i(x,t) - \frac{1}{\tau}[f_i(x,t) - f_i^{\mathrm{eq}}(x,t)] \tag{1}$$

where $\tau$ is the relaxation time (dimensionless). Eq. (1) implies the collisions redistribute the distribution function towards equilibrium state $f_i^{\mathrm{eq}}$ with change a rate of $1/\tau$. And then, fluid particles migrate to a nearest node with position $\mathbf{x}$ along the direction $i$ ($\mathbf{x} + \mathbf{c}_i\Delta t$):

$$f_i(x + \mathbf{c}_i\Delta t, t + \Delta t) = f_i^+(x,t) \tag{2}$$

Combined Eqs. (1) and (2), the evolution equation of $f_i(\mathbf{x},t)$ can be written as following:

$$f_i(x + \mathbf{c}_i\Delta t, t + \Delta t) - f_i(x,t) = \frac{1}{\tau}[f_i^{\mathrm{eq}}(x,t) - f_i(x,t)] \tag{3}$$

Eq. (3) indicates the difference of the original $f_i(\mathbf{x},t)$ and the streamed $f_i(\mathbf{x} + \mathbf{c}_i\Delta t, t + \Delta t)$ is related to the changes due to collisions during the motion of the fluid particles. The equilibrium distribution function $f_i^{\mathrm{eq}}$ is calculated as follows:

$$f_i^{\mathrm{eq}} = \rho\alpha_i\left[1 + \frac{\mathbf{c}_i\cdot\mathbf{u}}{c_s^2} + \frac{1}{2}\left(\frac{\mathbf{c}_i\cdot\mathbf{u}}{c_s^2}\right)^2 - \frac{\mathbf{u}^2}{2c_s^2}\right] \tag{4}$$

where $\alpha_i$ is the fixed weighting coefficient related to the model, here $\alpha_0 = 4/9$, $\alpha_i = 1/9$ ($i = 1,3,5,7$), $\alpha_i = 1/36$ ($i = 2,4,6,8$); $c_s$ is the local sound speed, $c_s = \sqrt{3}c/3$; $c = \Delta x/\Delta t$; $\Delta x$ is the grid length (in the *D*2*Q*9 model both $x$- and $y$-directions are with the same sampling $\Delta x$).

By performing the streaming step and the collision step successively at each grid point, the LB algorithm proceeds to obtain the gas flow and potential fields. The pressure of a discrete node is calculated as:

$$P = \rho c_s^2 \tag{5}$$

and the macroscopic density $\rho$ and momentum $\rho\mathbf{u}$ of fluids can be calculated as the first two moments of $f_i$:

$$\rho = \sum_{i=0}^{Q-1} f_i, \quad \rho\mathbf{u} = \sum_{i=0}^{Q-1} f_i\mathbf{c}_i \tag{6}$$

where $Q$ is the number of discrete velocities (here $Q = 9$).

The LB method represents a first-order explicit finite-difference discretization of the finite discrete velocity model of the Boltzmann equation [24]. It is well known from the kinetic theory of gases that the Navier–Stokes equations usually used in macroscopic simulation are solutions of the Boltzmann equation in the continuum regime [25]. Consequently, Eq. (3) can correctly reproduce the incompressible Navier–Stokes equations with second-order accuracy in space, giving the speed of sound *c*s and the kinematic viscosity of the fluid ($v$)

$$v = \frac{c_s^2}{2}(2\tau - 1)\Delta t \tag{7}$$

Although the LB method exhibits many advantages, it may suffer numerical instability for high Reynolds number turbulence. Fortunately, there are several methods to overcome the problem. One of them is to densify the computational nodes, which will expend more computational cost. Another is to reduce the effective relaxation time and then reduce the effective kinematic viscosity of the fluid. The Smagorinsky subgrid model [26,27] is introduced here into the LB model to simulate turbulence with high Reynolds number. The essential idea is to define a space-filtered fluid-particle density distribution function and to allow the dynamics of the filtered distribution function to have a space-dependent relaxation [28]. In the Smagorinsky subgrid model, the effective viscosity ($v_e$) is split as $v$ (the original viscosity given in Eq. (7) and $v_t$ (the turbulent viscosity resulting from the filtered scales):

$$v_e = v + v_t = c_s^2\cdot\Delta t\cdot(2\tau_e - 1)/2 \tag{8}$$

Eq. (8) means an effective relaxation time $\tau_e$ dependent on time and space is introduced to increase the local relaxation time $\tau$. In the Smagorinsky subgrid model $v_t$ is expressed as:

$$v_t = (C\delta)^2|S| \tag{9}$$

where $C$ is the Smagorinsky constant ($C = 0.05$ here); $\delta$ is the filter scale and related to the grid length (in this paper, $\delta = \Delta x$); $|S| = \sqrt{2S_{\alpha\beta}S_{\alpha\beta}}$ is the magnitude of the large scale strain rate tensor $S_{\alpha\beta}$ and $S_{\alpha\beta} = 1/2(\partial_\beta u_\alpha + \partial_\alpha u_\beta)$.

In the LB model, $|S|$ can be easily calculated using the nonequilibrium properties of the filtered fluid-particle density distribution function [26]:

$$|S| = \frac{\sqrt{v^2 + 18C\delta^2 Q^{1/2}} - v}{6C\delta^2} \tag{10}$$

where $Q = \Pi_{\alpha\beta}\Pi_{\alpha\beta}$, $\Pi_{\alpha\beta}$ is local nonequilibrium stress tensor, $\Pi_{\alpha\beta} = \sum_{i=0}^{8} c_{i\alpha}c_{i\beta}(f_i - f_i^{eq})$.

## 3. The cellular automata probabilistic model for the dispersed-phase dynamics

In the CA probabilistic model for particle transport, solid particles are constrained to only move on the same regular lattices as the fluid particles, and their transport probabilities to neighboring nodes depend on the local fluid flow and other external forces subject to solid particles. Let a particle locate at site $\mathbf{x}_p$ and time $t$. After a time-step $\Delta t$ its new position ($\mathbf{x}_p^*$) is $\mathbf{x}_p + \mathbf{u}_p\Delta t$, where $\mathbf{u}_p$ is the particle velocity at time $t$. It is noted that the time-step is constrained to be less than the crossing time scale of solid particle to the grid, in such a way that a solid particle moves to its nearest-neighbor node within $\Delta t$ at maximum. Usually the new position does not coincide with any node of the grid. The key idea of the CA probabilities model is to introduce the stochastic process to judge the next node of a solid particle after $\Delta t$. The probability $p_i$, which a solid particle at site $\mathbf{x}_p$ and time $t$ will jump to a neighboring node at site $\mathbf{x}_p + \mathbf{e}_i\Delta t$, is proportional to the projection of the actual displacement of the particle in the direction $\mathbf{e}_i$. Fig. 2 illustrates an example of the transport rule for the $D2Q9$ model. The transport probabilities of the particle awards to the east, north, west, and south direction, *i.e.*, $p_1$, $p_3$, $p_5$ and $p_7$, are calculated in the $D2Q9$ model:

$$p_i = \max\left(0, (\mathbf{u}_p \cdot \mathbf{e}_i)\frac{\Delta t}{\Delta x}\right) = \max\left(0, \frac{\Delta x_p}{\Delta x} \cdot \mathbf{e}_i\right), \quad i = 1, 3, 5, 7 \tag{11}$$

where $\Delta x_p$ is the actual displacement of the particle within time step $\Delta t$, $\Delta x_p = \mathbf{x}_p^* - \mathbf{x}_p = \mathbf{u}_p\Delta t$. It is clear that $p_i \times p_{i+4} = 0$ since $\mathbf{e}_i = -\mathbf{e}_{i+4}$.

The solid particle may still stay at the original node or jump to a nearest-neighbor node, depending on the transport probabilities to direction 1, 3, 5 and 7:

$$\mathbf{x}_p^* = \mathbf{x}_p + \mu_1\mathbf{e}_1 + \mu_3\mathbf{e}_3 + \mu_5\mathbf{e}_5 + \mu_7\mathbf{e}_7 \tag{12}$$

where $\mu_i$ is a Boolean variable which is equal to 1 with probability $p_i$. Giving a typical example as shown in Fig. 2, where $p_1 > 0$, $p_3 > 0$, $p_5 = 0$, and $p_7 = 0$. It means the particle may stay at rest with probability $(1-p_1)(1-p_3)$, or jump to east with probability $p_1(1-p_3)$, to north with probability $p_3(1-p_1)$, to north-east with probability $p_1p_3$. As for numerical implementation, two independent random number from a uniform distribution in the interval [0,1], $r_1$ and $r_2$, are first generated through random number generator. The following conditions are used to determine the new position of the particle by Monte Carlo method:

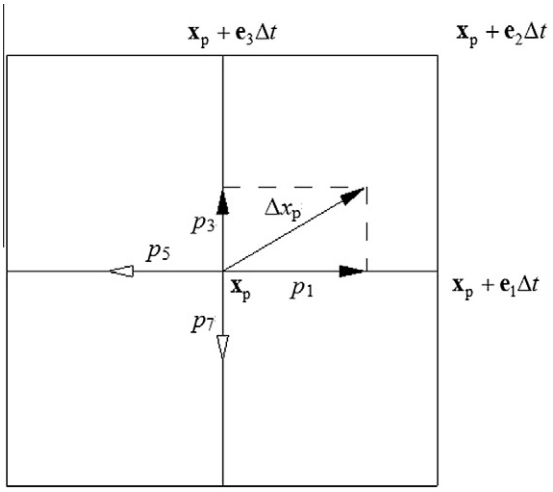


**Fig. 2.** Particle motion rule of CA probabilistic model.

$$\begin{cases} \text{if } r_1 > p_1 \text{ and } r_2 > p_3,\ \mathbf{x}_p^* = \mathbf{x}_p \\ \text{if } r_1 < p_1 \text{ and } r_2 > p_3,\ \mathbf{x}_p^* = \mathbf{x}_p + \mathbf{e}_1 \Delta t \\ \text{if } r_1 > p_1 \text{ and } r_2 < p_3,\ \mathbf{x}_p^* = \mathbf{x}_p + \mathbf{e}_3 \Delta t \\ \text{if } r_1 < p_1 \text{ and } r_2 < p_3,\ \mathbf{x}_p^* = \mathbf{x}_p + \mathbf{e}_2 \Delta t \end{cases} \tag{13}$$

It is proven that the binomial scattering can be approximated by a Gaussian distribution if the number of simulation particles is large enough [29].

The actual displacement $\Delta x_p$ can be quantitatively calculated by the Lagrangian approach of the equation of motion. The particle motion can be described by the Newtonian equation under consideration of external forces:

$$\frac{d\mathbf{u}_p}{dt} = \mathbf{F}_{drag} + \mathbf{F}_{buo} + \mathbf{F}_g + \mathbf{F}_{other} \tag{14}$$

where $\mathbf{F}_{drag}$ is the drag force, $\mathbf{F}_{buo}$ is buoyancy force, $\mathbf{F}_g$ is gravity, and $\mathbf{F}_{other}$ represents other external forces such as Saffman force, Magus force and Brownian force. In this paper, only drag force, buoyancy force and gravity are taken into account, so the governing equation can be written as:

$$\frac{d\mathbf{u}_p}{dt} = \frac{\mathbf{u} - \mathbf{u}_p}{\tau_p} + \left(1 - \frac{\rho}{\rho_p}\right)\mathbf{g} \tag{15}$$

where $\mathbf{u}_p$ is the particle velocity; $\tau_p$ is the relaxation time scale of particle, $\tau_p = \rho_p d_p^2/(18\mu)$; $\mu$ is the dynamic viscosity of gas; $d_p$ and $\rho_p$ are particle diameter and density respectively; $\mathbf{g}$ is gravity acceleration. The particle velocity and displacement after the $n$th time-step $\Delta t$ can be explicitly calculated through twice integration of Eq. (15) over time $t$:

$$\mathbf{u}_p^* = \mathbf{u}_p \cdot \exp\left(-\frac{\Delta t}{\tau_p}\right) + \left(\mathbf{u} + \left(1 - \frac{\rho}{\rho_p}\right)\mathbf{g} \cdot \tau_p\right) \cdot \left(1 - \exp\left(-\frac{\Delta t}{\tau_p}\right)\right) \tag{16}$$

$$\mathbf{x}_p^* = \mathbf{x}_p + (\mathbf{u}_p - \mathbf{u})\left(1 - \exp\left(-\frac{\Delta t}{\tau_p}\right)\right) + \mathbf{u}\Delta t + \left(\Delta t + \left(1 - \exp\left(-\frac{\Delta t}{\tau_p}\right) \cdot \tau_p\right)\right) \cdot \left(1 - \frac{\rho}{\rho_p}\right)\mathbf{g} \cdot \tau_p \tag{17}$$

The actual particle displacement $\Delta x$ ($=\mathbf{x}_p^{n+1} - \mathbf{x}_p^n$) during the period $\Delta t$ is thus obtained.

The present CA probabilistic model is able to consider particle transport under the action of other external forces such as electrical forces and van der Waals forces, by adding these forces into Eq. (15). It is also possible to take into account particle rotation by angular velocity of particles, if necessary.

Once the particle position and velocity are determined by the LB-CA model, the particle fields can be obtained by counting all simulation particles over all nodes. Simulation particles are usually weighted to represent these real particles. Let $N(\mathbf{x},t)$ be the number of simulation particles at site $\mathbf{x}$ and time $t$. $N(\mathbf{x},t)$ can take any nonnegative value. The number, $N_r(\mathbf{x},t)$, of real particles at site $\mathbf{x}$ and time $t$ can be calculated by: $N_r(\mathbf{x},t) = \sum_{i=1}^{N(\mathbf{x},t)} w_i$; the velocity, $\mathbf{u}_p(\mathbf{x},t)$, of real particles is given by $\mathbf{u}_p(\mathbf{x},t) = \sum_{i=1}^{N(\mathbf{x},t)} w_i \mathbf{u}_{p,i}$; and other variables of particle fields can be calculated using the similar ways, where $w_i$ and $\mathbf{u}_{p,i}$ are the weight and velocity of the $i$th simulation particle at site $\mathbf{x}$ and time $t$. In this paper monodispersed particles are considered and each simulation particle represents a real particle, $w_i = 1$.

## 4. The two-way coupling in the LB-CA method

According to the volume fraction ($\Phi_v$) occupied by particles, the interphase coupling can be divided into three levels [4]: one-way coupling ($\Phi_v < 10^{-6}$, the feedback forcing of particles on fluid dynamics can be neglected), two-way coupling ($10^{-6} < \Phi_v < 10^{-3}$, the interaction between fluid and particles must be considered) and four-way coupling ($\Phi_v > 10^{-3}$, besides interaction between fluid and particles, collision among particles should be included) [30]. In this paper, we consider the two-way coupling in the LB-CA method. The key issue is to find a way to couple the feedback forcing of particles acting on the flow field. In the LB method, we can add an external force term in the evolution equation of distribution function to realize the interphase coupling [31,32]:

$$f_i(x + e_i\Delta t, t + \Delta t) - f_i(x,t) = \frac{1}{\tau}[f_i^{eq}(x,t) - f_i(x,t)] + F_i \cdot \Delta t \tag{18}$$

$$F_i = 3\alpha_i e_i \cdot F/c \tag{19}$$

where $F_i$ represents the counterforce of solid particles on fluid particles; the force term $F$ is derived from the transfer of momentum between the two phases, $F = -\frac{\rho_p}{\rho} V_r \sum_{k=1}^{M} F_{pk}$; $M$ is the number of solid particles within the control volume; $V_r$ is the ratio of one particle volume to control volume, $V_r = \frac{\pi}{6}(\frac{d_p}{dx})^3$; $\mathbf{F}_{pk}$ is the external forces acting on the particle $k$, $\mathbf{F}_{pk} = \frac{d\mathbf{u}_p}{dt} = \frac{\mathbf{u}_f - \mathbf{u}_p}{\tau_p}$. Actually, the particle–fluid interaction is developed into the particle source in cell (PSIC) method. Through the Chapman–Enskog expansion, the macroscopic Navier–Stokes equation can be derivated from Eq. (18):

$$\frac{\partial \mathbf{u}}{\partial t} + \nabla \cdot (\mathbf{u}\mathbf{u}) = -\nabla p + \mathrm{Re}^{-1}\nabla^2 \mathbf{u} + \mathbf{F} \tag{20}$$

It is worth noting that, in the two-way coupling LB-Lagrangian method **F** is usually distributed linearly to grid nodes which surround the control volume according to the distance between a solid particle and a grid node [11]. This may lead to the complexity of numerical method and to numerical error because of the linear distribution. Differently, in the LB-CA method solid particles move in the same grids as fluid particles, in such a way that it is easy to calculate the feedback force of solid particles on fluid particles at each grid node. So, the LB-CA method is at advantage of the convenient implementation of the two-way coupling.

## 5. Boundary conditions

The inlet velocity of flow field is invariable: in laminar flow, the velocity profile satisfies parabolic distribution; in turbulent flow, gas flow enters the inlet with a 1/7th power velocity profile. In the outlet, the flow field is fully developed ($\frac{\partial u}{\partial x} = \frac{\partial v}{\partial x} = 0$) for all cases. Other boundaries are regarded as non-slip boundaries. Non-equilibrium extrapolation scheme is introduced to deal with the boundary conditions [33]. The principle of this scheme is to decompose the distribution function at the boundary node into its equilibrium and non-equilibrium parts and then to approximate the non-equilibrium part with a first-order extrapolation of the non-equilibrium part of the distribution at the neighboring fluid node [34]:

$$f_i(\mathbf{x}_b) = f_i^{eq}(\mathbf{x}_b) + [f_i(\mathbf{x}_f) - f_i^{eq}(\mathbf{x}_f)] \tag{21}$$

where $\mathbf{x}_f$ is the nearest neighbor fluid node of boundary node $\mathbf{x}_b$ ($\mathbf{x}_f = \mathbf{x}_b + \mathbf{e}_i\Delta t$).

The collision between solid particles and wall is another problem needed to be solved reasonably. In this paper, we assume that the collision is perfect elastic collision and mirror reflection occurs during the particle–wall collision process.

## 6. Numerical simulations of backward-facing step flows

### 6.1. The LB method for flow field

With the increase of Reynolds number ($Re = UD/\nu$, $U$ is two-thirds of the maximum inlet velocity, $D$ is the hydraulic diameter of the inlet channel) the backward-facing step flows develop from laminar flow ($Re < 1200$) to transitional flow ($1200 < Re < 6600$), and finally to turbulent flow ($Re > 6600$) [35]. The variations of the reattachment length and separation length are significant characteristics for various flow regimes. Armaly et al. [35] reported the Laser-Doppler measurements of characteristic lengths as a function of $Re$. In this section, we investigated the variations of characteristic lengths with $Re$ that covers the three different regimes of flow by the LB subgrid model for high Reynolds-number flows, and compare numerical results with experimental measurements, as shown in Fig. 3. The grid resolution is $50 \times 750$. The inlet of flow field is treated as velocity boundary with a parabolic velocity profile and outlet is regarded as fully developed, other wall boundaries are non-slip boundaries. In the laminar regime, the reattachment length $x_1$ increases with $Re$. In the transitional regime ($1200 < Re < 6600$), the reattachment length first decreases sharply, then decreases gradually and irregularly to a minimum value at $Re$ of about 5500, then increases gradually to a steady value at $Re$ of about 6600. Afterwards the reattachment length $x_1$ will not change with $Re$ throughout the turbulent-flow regime. When $Re$ is higher than approximately 400, an additional recirculation-flow region appears near the upper wall downstream of the expansion. The recirculation area moves to the in-

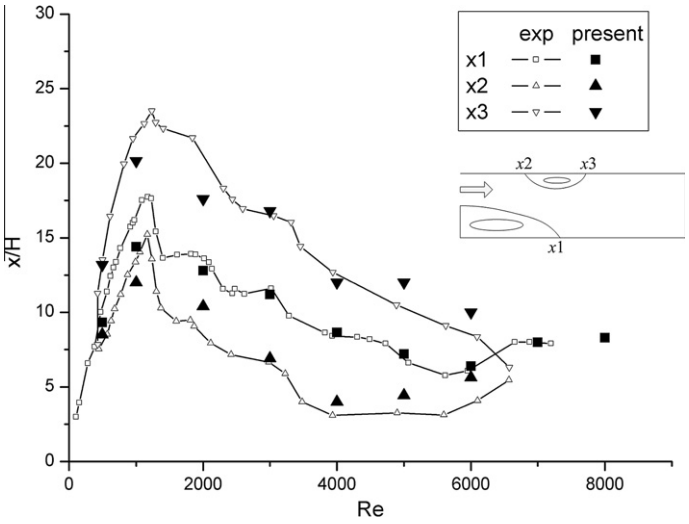


**Fig. 3.** Relationship between length of reattachment and $Re$.

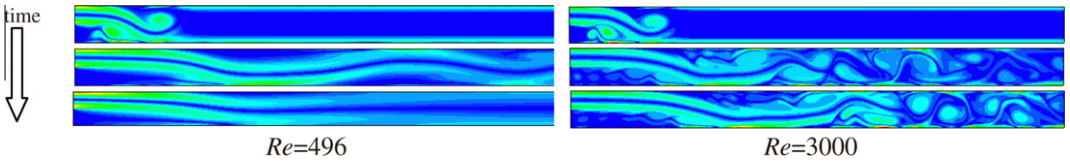


**Fig. 4.** Vortex evolution for different *Re* number.

let and oppress the length of the first reattachment with increase of *Re*. When flow regime gets into turbulent flow ($Re > 6600$), the recirculation area disappears. As presented in Fig. 3, the LB results agree well with the experimental results. There are a few differences between the two results, especially for higher *Re*. The possible reason is the experiment could not exactly achieve two-dimensionality. Fig. 4 presented the evolution of turbulent vortex for $Re = 496$ and 3000. It can be found that the flow field achieves stable state in the laminar regime however keeps fluctuating in the transitional regime.

### 6.2. The CA probabilistic model for particle motion

In order to verify the validity and accuracy of the CA probabilistic model for particle motion, we further examined particle trajectory and compared the results from the LB-CA method and the LB-Lagrangian method respectively. Here a dilute gas-particle flow over a backward-facing step is simulated and the one-way coupling is considered for the two methods. Laminar flow ($Re = 496$) is chosen here for showing clear particle trajectories. Laminar flow field over a backward facing step has steady vortex structure without fluctuation. Expansion ratio is $h{:}H = 1{:}2$, $h$ is step height and $H$ is channel height. Length of channel is $30h$. Velocity of inlet is:

$$u(y) = u_{\max}\frac{y-h}{h}\left(1-\frac{y-h}{h}\right), \quad h \leqslant y \leqslant 2h \tag{22}$$

where $u_{\max}$ is the maximum velocity of inlet along the center line ($u_{\max} = 1.0$ here). Non-slip boundary condition ($u = v = 0$) is realized, and the channel outlet is regarded as fully developed. The grid resolution of $50 \times 750$ is used.

The LB-Lagrangian and LB-CA methods are used to calculate the particle trajectories and particle velocity profiles. Fig. 5 presents the schematic of the two models for particle motion from node A to node D (A → B → C → D). In the LB-Lagrangian method, the particle motion is governed by the Newtonian equation and the particle trajectories are explicitly determined, where the particle position at a time does not usually correspond to a grid node. Bilinear interpolation is used to distribute the forces acting on particles to neighboring four grid nodes in order to consider the interphase interaction [11]. The LB-CA model also uses the Newtonian equation to determine the particle transport probability among neighboring nodes, and solid particles only move within the regular lattices. As a result, the feedback forcing from external forces of solid particles at each node can be easily obtained, and the two-way coupling can be easily realized.

Fig. 6 presented particle trajectories of four particles injected from the specified positions of the inlet (numbered by part1–4). Particles near the step fall into the recirculation region because of low initial velocity and gravity, their trajectories gradually close to the step (e.g., part1). Other particles are also affected by the drag force and gravity, some of them could move to the outlet (part3 and part4) and some would collide with wall (for example, part2). Parameters which affect particle trajectory are mainly Stokes number (*St*), *Re*, and so on. In this part, what we concern about is the accuracy of LB-CA method. It is obvious that the results from the LB-CA method are in close agreement with these from the LB-Lagrangian method. Generally, the particle trajectories from the LB-CA method fluctuate slightly, however the LB-Lagrangian method produces relatively regular particle trajectories. The deviations are explainable by the inherent randomicity of the LB-CA method for determining the particle position.

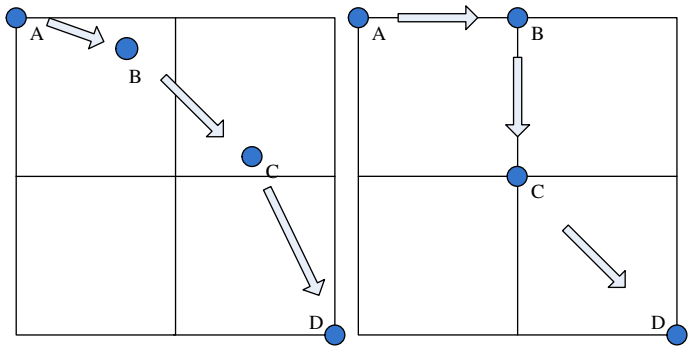


**Fig. 5.** The schematic of the LB-Lagrangian and LB-CA methods for particle motion (left: the LB-Lagrangian method; right: the LB-CA method).

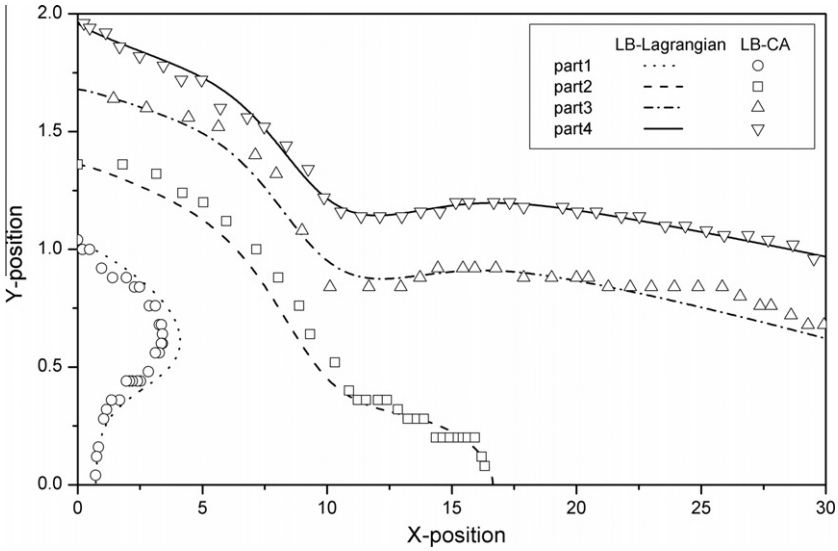


**Fig. 6.** Trajectories of four specific particles ($Re = 496$).

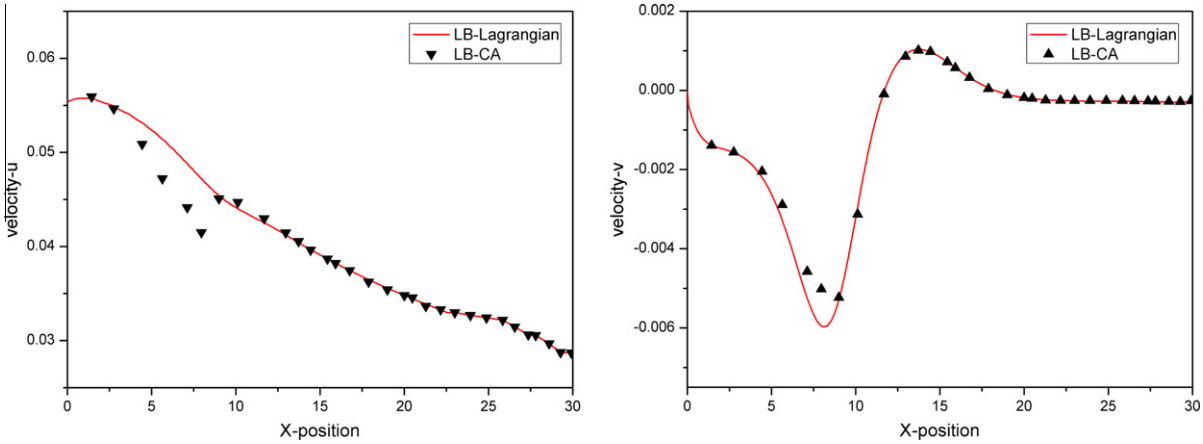


**Fig. 7.** Velocity profiles of the third particle in $x$- and $y$-directions (part3).

Fig. 7 presented the variation of particle velocity (for part3) when carried by the fluid. Particle velocity of the wall-normal direction changes more than that of the streamwise due to the presence of turbulence vortex. By comparison with the LB-Lagrangian method, not only particle trajectories but also velocity variations obtained from the LB-CA model have achieved high precision. In the LB-CA method, particles always locate at the grid nodes and the particle trajectories are thus not so smooth. This also leads to the deviation in particle velocity profile, especially in the region where flow velocity field changes remarkably (for example, $5 < x < 10$, where the reattachment region of upper boundary exists).

### 6.3. The LB-CA method for gas-particle flows

The gas-particle two-phase flows basically belong to turbulence, and the simulation of two-phase turbulent flows is one of the most challenging topics in fluid mechanics. Besides the randomness of turbulence, the presence of particles may strengthen the randomness, which makes the simulation of gas-particle turbulent flows much more complex than for laminar flows. In fact, small particle ($d < \eta$, $d$ is particle diameter scale, and $\eta$ the Kolmogorov length scale) can be treated as mass point, while for large particle ($d \geqslant \eta$) the gas-particle turbulence model must consider the size of particles and trailing vortex behind particles [4]. For this case the solid particle is viewed as point-like small particle. In this section, the LB-CA method is used to simulate the gas-particle turbulent flow over a backward-facing step, and the numerical results are compared with the classical experiment by Fessler and Eaton [36]. Computational domain is presented in Fig. 8. The expansion ratio of backward-facing step is 5:3. The Reynolds number is 18,400, based on the step height $H = 26.7$ mm, and the gas velocity at center

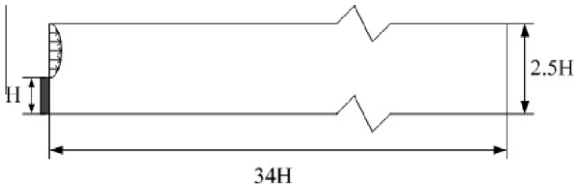


**Fig. 8.** Computational region of back-facing step flow.

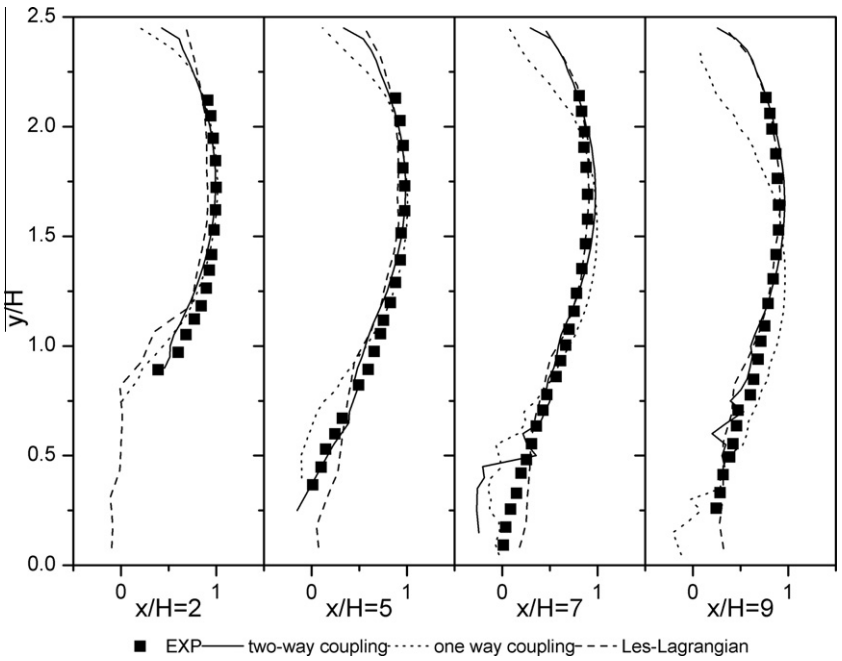


**Fig. 9.** 70 μm copper streamwise mean velocities ($\bar{u}_p/U_0$).

line of the inlet $U_0$ = 10.5 m/s, the length of channel is 34$H$. A two-dimension grid of 50 × 680 is used here. Particles injected in the flow field is copper particles with diameter $d_p$ = 70 μm, density $\rho_p$ = 8800 kg/m$^3$ and mass loading of 0.1–0.4.

*6.3.1. Dispersed phase*

Fig. 9 presents the streamwise mean velocities of 70 μm copper particles at several specified cross sections ($x/H$ = 2, 5, 7, 9). Obviously, the results of two-way coupling model agree with experimental data better. The particle velocity profile is similar with the gas velocity profile (which will be shown in Section 6.3.2). In the separation region attached to the step ($x/H$ = 2, 5), the results of two-way coupling are in closer agreement to the experimental measurements. The particle velocities of two-way coupling are generally larger than these of one-way coupling in the recirculation-flow region near the upper wall downstream of the expansion, and the deviation of particle velocity between the two models is larger than that of gas velocity between the one-way coupling and two-way coupling. In the mainstream region, the particle velocities of two-way coupling is generally less than that of one-way coupling, and the deviation of two kinds of particle velocities is less than that of two kinds of gas velocities. In the reattachment region near lower boundary, both results from the one-way and two-way coupling models show more fluctuations and deviate slightly from the experimental results. That is because fewer particles can be entrained in the reattachment region, and then statistical noise arises due to the lack of sample (i.e., simulation particle) number. Comparing the gas velocity and particle velocity in streamwise direction, one can find that the particle velocity profile changes more gently, which means that the vortex intensity of turbulent flow is weakened due to the interaction between particles and fluid. It coincides with the classic conclusion of "small particles attenuate turbulence however large particles strengthen turbulence" [37.38].

Fig. 10 presents particle fluctuating velocities. The agreement between the results from the LB-CA method (with the two-way coupling) and experimental data is good on the whole. There are obvious differences for streamwise fluctuating velocities at $x/H$ = 2 and $x/H$ = 5, because the particles are injected in the flow field with pre-specified velocity (95% of local fluid velocity) and have not fully developed in the region close to the inlet ($x/H$ = 2,5 and $y/H$ > 1); Another reason is that there are

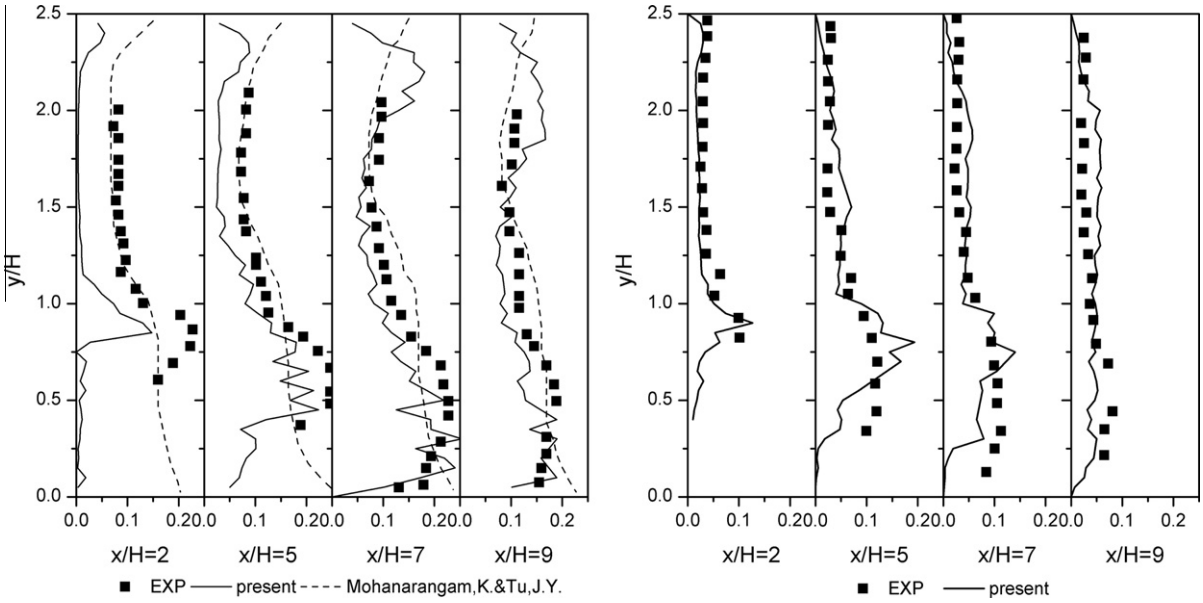


**Fig. 10.** Fluctuating velocities of particles (left: streamwise, $u'_p/U_0$; right: wall-normal, $v'_p/U_0$).

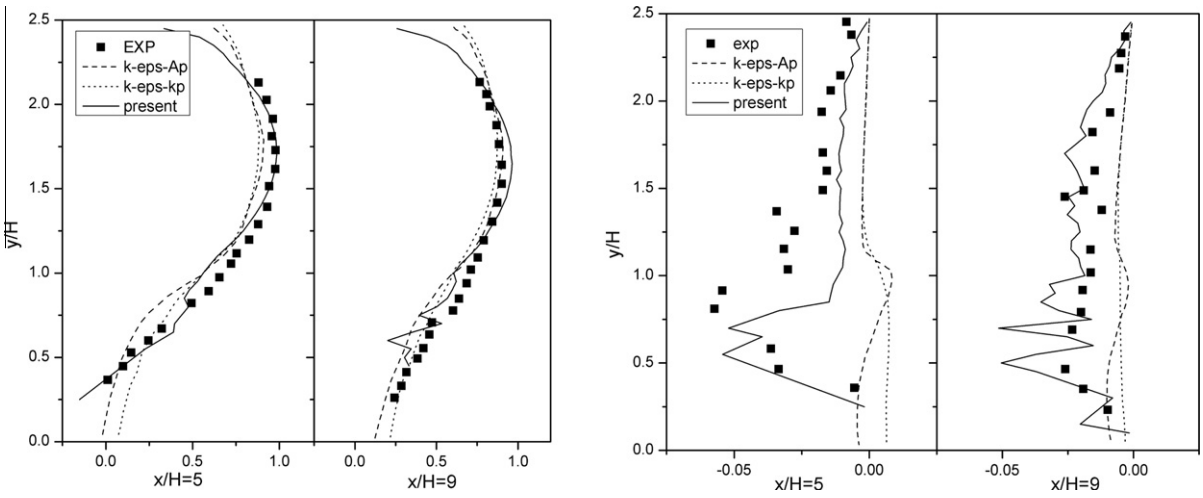


**Fig. 11.** Particle mean velocities, compared with two different two-fluid models (left: streamwise, $\bar{u}_p/U_0$; right: wall-normal, $\bar{v}_p/U_0$).

few particles entering into the region ($x/H = 2{,}5$ and $y/H < 1$) and the statistical results are thus underestimated and show obvious fluctuations. It is also can be found that the particle wall-normal fluctuating velocities agree well with the experimental data, which are rarely reported by other investigations.

Several researchers simulated the same case using different multiphase models. Yu et al. [39] used the LES (large-eddy simulation)-Lagrangian model to simulate Fessler and Eaton's experiment. Fig. 9 shows the streamwise mean velocities of particles obtained from the LES-Lagrangian and LB-CA models. Generally speaking, the two models predict the particle velocity profile with nearly same precision. Fesslor & Eaton also used the two-fluid model to simulate their experiment. Fig. 11 presents the comparison between the LB-CA model and two kinds of two-fluid models. There is nearly no differences for particle streamwise mean velocities among the three models. However, an obvious improvement can be found with respect to the wall-normal particle mean velocities.

Mohanarangam and Tu also used the two-fluid model to simulate the classic experiment and investigated the fluctuating velocity of particles. Fig. 10 presents the comparison between the two-fluid model by Mohanarangam and Tu [40] and the LB-CA model with regards to particle streamwise fluctuating velocities. The two-fluid model overestimated the fluctuating velocities in the regions near upper and lower boundary, and the variation trend of streamwise fluctuating velocities is also

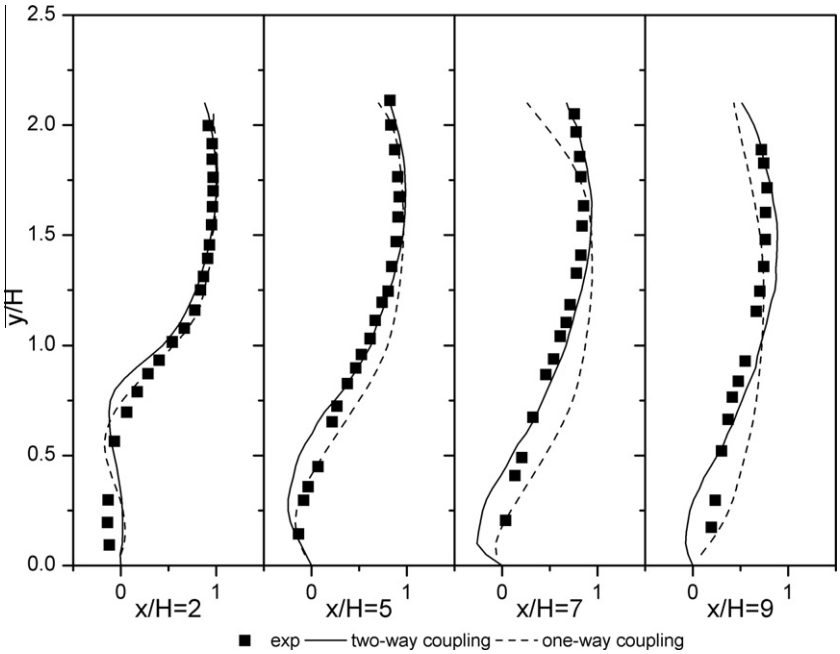


**Fig. 12.** Gas-phase streamwise mean velocities ($\bar{u}_f/U_0$) in presence of 70 μm copper particle.

obviously different from experimental data. The LB-CA model overcomes the problems and shows a better agreement with experimental data.

*6.3.2. Continuous phase*

Fig. 12 presents the mean streamwise gas-phase velocities in the presence of 70 μm copper particles. Vortex appears behind the step, and the streamwise gas velocity may become negative and the twin peaks structure is thus formed. One peak occurs around $y/H$ = 1.5–2.0 and another peak with opposite direction is around $y/H$ = 0.5. The recirculation region gradually disappears with the development of flow field and the twin peaks structure also disappears by degrees. Along the flow direction the region near lower boundary can be divided into corner vortex region, recirculation region and fully-developed region respectively. There exists no additional recirculation region near the upper wall downstream of the expansion.

On the whole, the results of two-way coupling simulation are in agreement with the experimental data [36]. On the contrary, there are obvious deviations between the results of one-way coupling and experimental data, especially in the vortex region near upper boundary($x/H$ = 7,9, $y/H$ > 1.5) and the mainstream region. It means that the feedback forcing of particles cannot be neglected in this case. The gas velocity of one-way coupling is less than that of two-way coupling in the region near upper boundary where vortex generates and develops. In fact, in the vortex region of upper boundary the motion direction of gas flow is forward on the whole but locally backward, and the feedback forcing of particles baffles the backflow to a certain extent. In the mainstream region and reattachment region, the gas velocity of one-way coupling is larger than that of two-way coupling, which can be explained by the bafflement effect of particles on gas flowing. Actually, particles gather near the lower boundary because of gravity and preferential accumulation led by the interaction of vortex and particles. The larger the particle concentration is, the more obvious the effect of feedback forcing is.

Fig. 13 presents the fluctuating velocities of gas-phase in presence of particles, which is rarely showed in other researches. For the fluctuating wall-normal gas velocities, the numerical results (the two-way coupling is considered) are in agreement with experimental data on the whole, while with respect to the fluctuating streamwise gas velocities there exist obvious difference between the LB-CA model and experimental measurements. The velocity boundary condition is used for the inlet, that is, the gas velocity at the inlet remain unchanged, which results in that the fluctuating gas velocity from the LB-CA model is obviously less than experimental data at the position $x/H$ = 2,5 and $y/H$ > 1.0, especially in the streamwise direction.

*6.3.3. Gas-particle covariance*

Gas-particle covariance is an important parameter in the multiphase flows, and it represents the interaction between the continuous phase and dispersed phase. Yu and Lee [41] investigated the gas-particle covariance to evaluate several second-order closure models through comparing their results with the results from the LES-Lagrangian model (which severs a benchmark). Different second-order closure models are represented by the following abbreviations:

PH: Pourahmadi and Humphrey's model [42], $\overline{u_g' u_p'} = 2k_g \frac{\tau_L}{\tau_p+\tau_L}$;

Chen: Chen and Wood's model [43], $\overline{u_g' u_p}' = 2k_g e^{(-B\tau_p/\tau_L)}$;

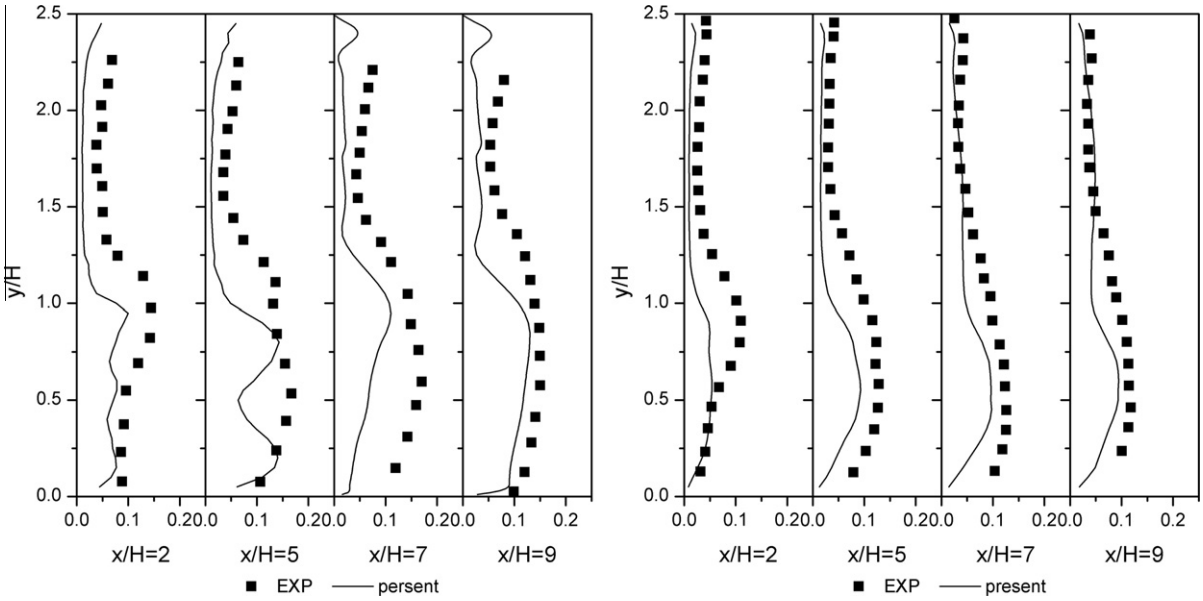


**Fig. 13.** Fluctuating velocities of fluid in presence of 70 μm copper particle (left: streamwise, $u'_f/U_0$; right: wall-normal, $v'_f/U_0$).

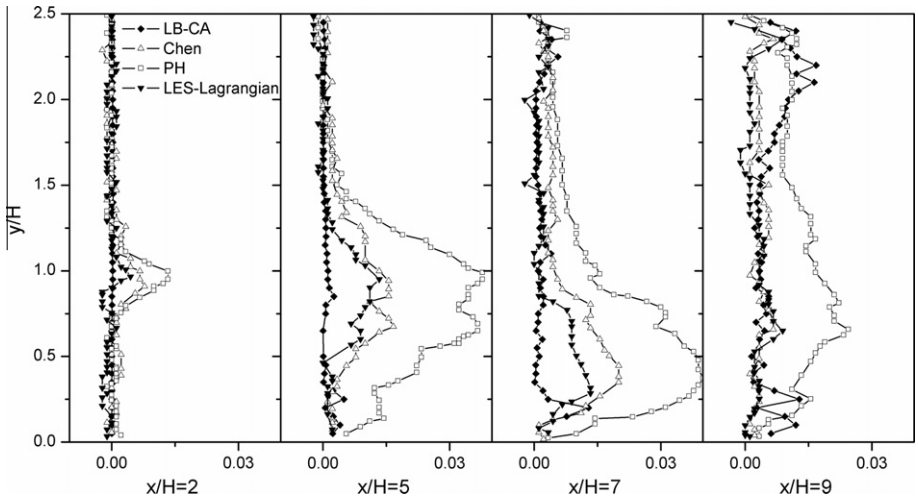


**Fig. 14.** $\overline{u'_f u'_p}$ calculated by different models.

where $k_g$ is the turbulent kinetic energy of gas phase, $\tau_p$ is the particle relaxation time, $\tau_L$ is the Lagrangian integral time scale of gas phase, and $B$ is an empirical constant.

In this section, the results from the LB-CA model and other three models are shown in the Fig. 14. If the LES results are viewed as the benchmark solution, the Chen model predicts $\overline{u'_f u'_p}$ very well, and the LB-CA model performs quite well, while the PH model obviously overestimates $\overline{u'_f u'_p}$. It should be pointed out that an empirical constant is needed in the Chen model for different cases (here $B = 0.5$). The results predicted by the LB-CA are better than the PH model, and are also in close agreement with these of the LES-Lagrangian model on the whole, although the LB results are smaller than the LES results at regions where $y/H = 0.5$–$1.5$ and $x/H = 2$–$7$ and larger than the LES results near the upper and lower boundary of $x/H = 9$.

## 7. Conclusions

This paper proposed the Lattice Boltzmann (LB)-cellular automata (CA) probabilistic model to simulate gas–solid turbulent flows at the mesoscopic level. The LB method is used to simulate the flow field, where the Smagorinsky subgrid model is

introduced to simulate turbulent flow at high Reynolds numbers. For a turbulent flow over backward-facing step, the LB method successfully captured the variations of the reattachment and separation lengths with Reynolds number (from the laminar, the transitional, to the turbulent regimes of flow). Particle motion is described by the CA probabilistic model, where point-like particles move only at the regular grid nodes as fluid particles, and the particle probabilistic position is determined by the random lattice gas rules in terms of transport probability (considering drag force, gravity and so on). The feedback forcing term is added into the evolution equation of fluid particle density distribution function to realize the two-way coupling. The resultant LB-CA method shows a good agreement with the conventional LB-Lagrangian method in the simulation of particle trajectory and velocity profile. The classical experiment of particle-laden flow over a backward-facing step is simulated by the LB-CA model. The mean and fluctuating velocities of the dispersed and carrier phases and the gas-particle covariance are obtained and compare with available experimental measurements and numerical results from the LES-Lagrangian model and the two-fluid models. It is found that the results of two-way coupling are better than these of one-way coupling, and the model presented in this paper captures well the interphase interaction and generally performs better than some other macroscopic models (such as the two-fluid models). Moreover, it can be concluded that the LB-CA method achieves the similar precision with the LES-Lagrangian method. What is noteworthy is that the LB-CA method, compared with other multiphase model based on the Navier–Stokes equations, is at advantages of clear physical picture, simplicity, intrinsic parallelism, and capability to deal with complex and dynamic boundary conditions. Furthermore, compared with other multiphase models based on the Lagrangian particle tracking, the LB-CA model is capable of considering easily the coupling between the two phases (because the solid particles and fluid particles use the same regular nodes) and capturing the fluctuating behaviors of the dispersed phase (because the particle transport between nodes are determined by stochastic processes).

## Acknowledgments

The authors were supported by "the National Natural Science Foundation of China" (50876037, 51021065), and "Program for New Century Excellent Talents in University" (NCET-10-0395), "National Key Basic Research and Development Program" (2010CB227004), and "State Key Laboratory of Multiphase Complex Systems" (MPCS-2011-D-02).

## Reference

[1] J.C.R. Hunt, Industrial and environmental fluid mechanics, Annu. Rev. Fluid Mech. 23 (1) (1991) 1–42.
[2] W.A. Sirignano, Fluid dynamics of sprays–1992 freeman scholar lecture, J. Fluids Eng. 115 (3) (1993) 345–378.
[3] S. Ghosh, J.C.R. Hunt, Induced air velocity within droplet driven sprays, Proc. R. Soc. London A 444 (1920) (1994) 105–127.
[4] S. Balachandar, J.K. Eaton, Turbulent dispersed multiphase flow, Annu. Rev. Fluid Mech. 42 (2010) 111–133.
[5] C. Chan, H. Zhang, K. Lau, Numerical simulation of gas-particle flows behind a backward-facing step using an improved stochastic separated flow model, Comput. Mech. 27 (5) (2001) 412–417.
[6] Y.H. Qian, D. D'Humières, P. Lallemand, Lattice BGK models for Navier–Stokes equation, Europhys. Lett. 17 (6) (1992) 479.
[7] A. Ladd, R. Verberg, Lattice-Boltzmann simulations of particle-fluid suspensions, J. Stat. Phys. 104 (5) (2001) 1191–1251.
[8] B. Chopard, A. Masselot, M. Droz, Multiparticle lattice gas model for a fluid: application to ballistic annihilation, Phys. Rev. Lett. 81 (9) (1998) 1845–1848.
[9] O. Filippova, D. Hänel, Lattice-Boltzmann simulation of gas-particle flow in filters, Comput. Fluids 26 (7) (1997) 697–712.
[10] U. Lantermann, D. Hänel, Particle Monte Carlo and lattice-Boltzmann methods for simulations of gas-particle flows, Comput. Fluids 36 (2) (2007) 407–422.
[11] S. Chen, B. Shi, Z. Liu, H. He, Z. Guo, C. Zheng, Lattice-Boltzmann simulation of particle-laden flow over a backward-facing step, Chin. Phys. 13 (2004) 1657.
[12] S. Chen, Z. Liu, B. Shi, C. Zheng, Computation of gas-solid flows by finite difference Boltzmann equation, Appl. Math. Comput. 173 (1) (2006) 33–49.
[13] A.J.C. Ladd, Short-time motion of colloidal particles: numerical simulation via a fluctuating lattice-Boltzmann equation, Phys. Rev. Lett. 70 (9) (1993) 1339–1342.
[14] A. Dupuis, B. Chopard, Lattice gas modeling of scour formation under submarine pipelines, J. Comput. Phys. 178 (1) (2002) 161–174.
[15] M. Chopard, A lattice Boltzmann model for particle transport and deposition, Europhys. Lett. 42 (3) (1998) 259–264.
[16] B. Chopard, A. Masselot, Cellular automata and lattice Boltzmann methods: a new approach to computational fluid dynamics and particle transport, Future Gener. Comput. Syst. 16 (2–3) (1999) 249–257.
[17] B. Chopard, A. Masselot, A. Dupuis, A lattice gas model for erosion and particles transport in a fluid, Comput. Phys. Commun. 129 (2000) 167–176.
[18] B. Chopard, M. Droz, Cellular Automata Modeling of Physical Systems, Cambridge University Press, Cambridge, UK, 1998.
[19] U. Frisch, B. Hasslacher, Y. Pomeau, Lattice-gas automata for the Navier–Stokes equation, Phys. Rev. Lett. 56 (14) (1986) 1505–1508.
[20] R. Przekop, A. Moskal, L. Gradoń, Lattice-Boltzmann approach for description of the structure of deposited particulate matter in fibrous filters, J. Aerosol Sci. 34 (2) (2003) 133–147.
[21] R. Przekop, L. Gradoń, Deposition and filtration of nanoparticles in the composites of nano- and microsized fibers, Aerosol Sci. Technol. 42 (6) (2008) 483–493.
[22] H. Wang, H. Zhao, Z. Guo, C. Zheng, Numerical simulation of particle capture process of fibrous filters using lattice Boltzmann two-phase flow model, Powder Technol. 227 (2012) 111–122.
[23] P.L. Bhatnagar, E.P. Gross, M. Krook, A model for collision processes in gases. I. Small amplitude processes in charged and neutral one-component systems, Phys. Rev. 94 (3) (1954) 511–525.
[24] C.K. Aidun, J.R. Clausen, Lattice-Boltzmann method for complex flows, Annu. Rev. Fluid Mech. 42 (2010) 439–472.
[25] T. Abe, Derivation of the lattice Boltzmann method by means of the discrete ordinate method for the Boltzmann equation, J. Comput. Phys. 131 (1) (1997) 241–246.
[26] H. Yu, L.S. Luo, S.S. Girimaji, LES of turbulent square jet flow using an MRT lattice Boltzmann model, Comput. Fluids 35 (8–9) (2006) 957–965.
[27] A. Dupuis, B. Chopard, Lattice gas modeling of scour formation under submarine pipelines, J. Comput. Phys. 178 (1) (2002) 161–174.
[28] S. Hou, J. Sterling, S. Chen, G.D. Doolen, A lattice Boltzmann subgrid model for high Reynolds number flows, Fields Inst. Commun. 6 (1996) 151–166.
[29] B. Chopard, L. Frachebourg, M. Droz, Multiparticle lattice gas automata for reaction diffusion systems, Int. J. Mod. Phys. C 5 (1) (1994) 47–64.
[30] S. Elghobashi, On predicting particle-laden turbulent flows, Appl. Sci. Res. 52 (4) (1994) 309–329.

[31] H. Yu, S.S. Girimaji, L.S. Luo, DNS and LES of decaying isotropic turbulence with and without frame rotation using lattice Boltzmann method, J. Comput. Phys. 209 (2) (2005) 599–616.
[32] H. Yu, L.S. Luo, S.S. Girimaji, LES of turbulent square jet flow using an MRT lattice Boltzmann model, Comput. Fluids 35 (8) (2006) 957–965.
[33] Z. Guo, C. Zheng, B. Shi, Discrete lattice effects on the forcing term in the lattice Boltzmann method, Phys. Rev. E 65 (4) (2002) 046308.
[34] Z. Guo, T.S. Zhao, Explicit finite-difference lattice Boltzmann method for curvilinear coordinates, Phys. Rev. E 67 (6) (2003) 066709.
[35] B. Armaly, F. Durst, J. Pereira, Experimental and theoretical investigation of backward-facing step flow, J. Fluid Mech. 127 (1) (1983) 473–496.
[36] J.R. Fessler, J.K. Eaton, Turbulence modification by particles in a backward-facing step flow, J. Fluid Mech. 394 (1999) 97–117.
[37] G. Hetsroni, Particles-turbulence interaction, Int. J. Multiphas. Flow 15 (5) (1989) 735–746.
[38] R. Gore, C. Crowe, Modulation of turbulence by a dispersed phase, J. Fluids Eng. 113 (2) (1991) 304–307.
[39] K.F. Yu, K.S. Lau, C.K. Chan, Numerical simulation of gas-particle flow in a single-side backward-facing step flow, J. Comput. Appl. Math. 163 (1) (2004) 319–331.
[40] K. Mohanarangam, J.Y. Tu, Two-fluid model for particle-turbulence interaction in a backward-facing step, AIChE J. 53 (9) (2007) 2254–2264.
[41] K.F. Yu, E.W.M. Lee, Evaluation and modification of gas-particle covariance models by large eddy simulation of a particle-laden turbulent flows over a backward-facing step, Int. J. Heat Mass Transfer 52 (23–24) (2009) 5652–5656.
[42] F. Pourahmadi, J. Humphrey, Modeling solid-fluid turbulent flows with application to predicting erosive wear, PhysicoChem. Hydrodyn. 4 (1983) 191–219.
[43] C. Chen, P. Wood, Turbulence closure modeling of the dilute gas-particle axisymmetric jet, AIChE J. 32 (1) (1986) 163–166.